Comparison of geometrical mapping for ring diagram analysis

Amel Zaatri [1,2], Thierry Corbard [2], Markus Roth [3], Irene González Hernández [4] and Oskar von der Lühe [1]

[1]Kiepenheuer-Institut für Sonnenphysik, Freiburg, Germany
[2]Département Cassiopée, Observatoire de la Côte d'Azur, Nice , France
[3]Max-Planck-Institute für Sonnensystemforschung, Katlenburg-Lindau, Germany
[4]National Solar Observatory, Tucson, USA

E-mail: amel@kis.uni-freiburg.de, corbard@oca.eu, roth@mps.mpg.de, irenegh@noao.edu, ovdluhe@kis.uni-freiburg.de

Abstract. Mapping the solar surface is a crucial step in any local helioseismology technique. Because the acoustic waves propagate along great circles at the solar surface, it has been shown that these circles need to be used in the geometrical construction of the plane grid. We study different types of projections based on great circles for the calculation of sub-surface flows from ring diagram analysis of GONG data. Azimuthal equidistant projection, transverse cylindrical projection, gnomonic projection and stereographic projection produce almost the same velocity fields with standard patch sizes ($15^\circ \times 15^\circ$). The difference between the four projections is more noticeable when larger patches ($30^\circ \times 30^\circ$) are used.

1. Introduction

Local helioseismology analysis of high resolution Dopplergrams which are projected from the spherical solar surface onto a plane requires careful projection mapping of the sphere, in order to match heliographic coordinates (latitude and longitude) as precisely as possible with Cartesian image coordinates. Care has to be taken to match the plane coordinate system with geodesics on the solar surface, as acoustic waves propagate along them. A prominent method for detecting sub-surface velocity fields is ring diagram analysis, where frequency shifts of maxima in the three-dimensional power spectra of the Doppler signal within a limited area on the solar surface are analyzed [1]. Within such an area, acoustic waves are treated as plane waves.

The local analysis requires an accurate determination of the heliographic position at each position in the Dopplergram, and solar rotation needs to be corrected for. Two projection algorithms which are based on great circles are used today. The remapping/tracking code of GONG++ ring diagram analysis is based on the transverse cylindrical projection [2], whereas in [3], ring diagram analysis of MDI data is based on the azimuthal equidistant projection, also called Postel projection. As we show in this paper, many projections based on the great circle principle can be used to map the solar surface. However, none of the existing projections is able to avoid distance distortions in the two spatial directions of the plane map.

Different patch sizes have also been used in ring diagram analysis before. Whereas the standard patch size is $15^\circ \times 15^\circ$ [4], bigger patches ($30^\circ \times 30^\circ$) have been used in order to reach deeper sub-surface layers [5]. In this work, we investigate four great circles based projections

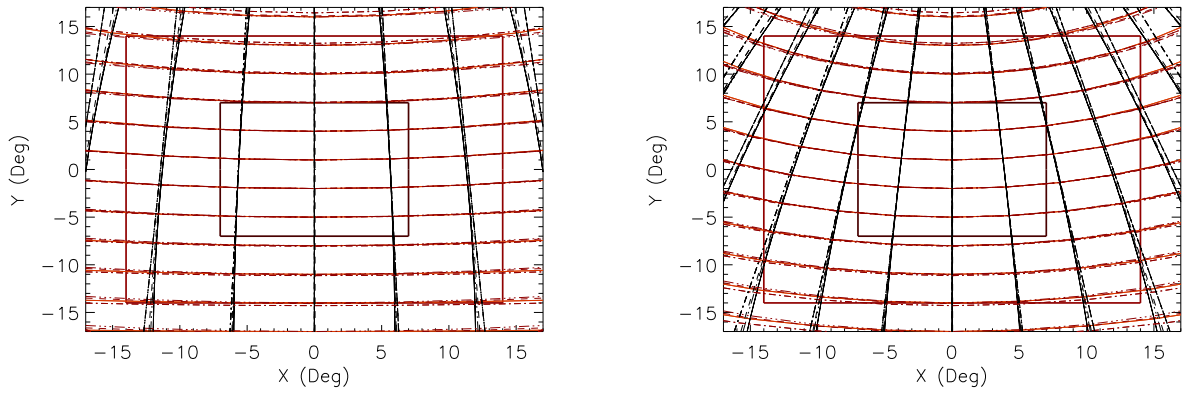

Figure 1. Geometrical maps obtained from the different projections studied here. Transverse cylindrical (full lines), Azimuthal equidistant (dotted), Stereographic (dashed), Gnomonic (dashed dotted). The left panel shows an area centered on the heliographic latitude $\theta_0 = 20°$, the right panel shows $\theta_0 = 50°$. Red lines are lines with same longitudes and black lines are the meridians. The two squares show the sizes of ring diagram analysis patches used here ($15° \times 15°$ and $30° \times 30°$).

(transverse equidistant cylindrical, azimuthal equidistant, stereographic and gnomonic) within areas of interest of various sizes. The daily velocity flows derived from each of these mappings, based on ring diagram analysis of two days of GONG++ data (02/01/2002 and 28/01/2002), are presented and compared.

2. Map projections

The most important criterion for selecting the appropriate mapping of the solar surface in ring diagram analysis is the use of great circles [6]. We describe in this section some of the projections that are generally based on great circles. The projections shown here are not the only possibilities. There are many good references on constructing geometrical maps, which are most frequently used to map the Earth; see for example [7].

All the described projections are presented for an arbitrary center of projection, defined by its heliographic latitude and longitude, $(\theta_0\ ,\ \phi_0)$. In the case of ring diagram analysis, this point corresponds to the center of the considered patch. If the latitude of the center of projection differs from zero, the projection is called "oblique". However, since most of the projections considered here are oblique we shall drop this term in the following to facilitate terminology.

2.1. Transverse cylindrical equidistant projection

The transverse cylindrical projection, also called Plate Carrée projection, is based on a cylinder projection surface where the central meridian is the tangent line between the cylinder and the sphere. The construction of this map can be done by rotating the original coordinate system, expressed in the heliographic latitude and longitude (θ, ϕ), such that the X axis points toward the center of the projection. In order to make the projection transverse, one needs to add a rotation which leads to inverting the roles of the equator and the central meridian. Then, the negative latitudes and the longitudes of the resulting coordinate system are taken as the X and Y Cartesian coordinates of the map. Consequently, all the great circles that are perpendicular to the central meridian at each point are mapped as horizontal lines, along which distances are preserved. However, distances along the vertical lines are not preserved except along the local

central meridian. The heliographic coordinates (θ, ϕ) as function of the Cartesian coordinates of the map are derived from the transformation equations

$$\theta = \arcsin\left(\cos X \sin\left(Y + \theta_0\right)\right), \qquad (1)$$
$$\phi = \arcsin\left(\frac{\sin X}{\cos\theta}\right) + \phi_0,$$

The plane grids which are generated from this projection when the center of projection is located at two different latitudes are shown in figure 1. This projection, as well as any of the other projections, produces a regular grid in a restricted central area of the solar disk where heliographic and Cartesian coordinates match well.

2.2. Azimuthal equidistant projection

The azimuthal cylindrical projection, also known as Postel projection, is based on a plane projection surface where the center of the projection is the tangent point between the sphere and the plane. This map can be constructed by pointing the Z axis towards the center of the projection. Then, the latitude and longitude of the resulting coordinate system are taken as the polar coordinates r and θ of the projection grid. Consequently, all the lines passing through the center of the projection in the map are great circles and distances are preserved along them. However, neither the Y direction nor the X direction of the map represent a real distance on the sphere. The heliographic coordinates (θ, ϕ) as function of the Cartesian coordinates of the map are derived from the transformation equations

$$\theta = \arcsin\left(\frac{Y}{r}\cos\theta_0 \sin r + \sin\theta_0 cosr\right), \qquad (2)$$
$$\phi = \arcsin\left(\frac{X}{r}\frac{\sin r}{\cos\theta}\right) + \phi_0,$$

where $r = \sqrt{X^2 + Y^2}$. The plane grid resulting from azimuthal equidistant projection is also shown in figure 1 for two latitudes of the center point.

2.3. Gnomonic projection

The Gnomonic projection uses the same rotations as the azimuthal equidistant projection, as the center of projection is also the pole of the resulting coordinate system. The Gnomonic projection is a perspective projection that takes the image of each point of the sphere as it is seen from the center of the sphere. In this projection, every line drawn in the resulting map is a great circle. However, the distance between any two points on the map is bigger than their real distance on the sphere, because of the perspective aspect. The heliographic coordinates (θ, ϕ) as function of Cartesian coordinates are

$$\theta = \arcsin\left(\frac{Y}{r}\cos\theta_0 \cos r_1 + \sin\theta_0 \sin r_1\right), \qquad (3)$$
$$\phi = \arcsin\left(\frac{X}{r}\frac{\cos r_1}{\cos\theta}\right) + \phi_0,$$

where $r = \sqrt{X^2 + Y^2}$ and $r_1 = \arctan(1/r)$. The Gnomonic projection map is almost the same as the the transverse cylindrical and the azimuthal equidistant maps for regions with the size of the standard patches. But the difference between the three projections becomes noticeable when using bigger patches (see figure 1).

2.4. Stereographic projection

The Stereographic projection is constructed in the same way as the azimuthal equidistant and the gnomonic projection. Thus, the center of projection is taken at the pole of a spherical coordinate system. The stereographic projection is a perspective projection that takes the image of each point as it is seen from the opposite point of the center of projection. In this projection, any straight line through the center of projection is a great circle. The heliographic coordinates (θ, ϕ) as function of the Cartesian coordinates map are

$$\theta = \arcsin\left(\frac{Y}{r}\cos\theta_0 \sin r_1 + \sin\theta_0 \cos r_1\right), \tag{4}$$

$$\phi = \arcsin\left(\frac{X}{r}\frac{\sin r_1}{\cos\theta}\right) + \phi_0,$$

where $r = \sqrt{X^2 + Y^2}$ and $r_1 = 2\arctan(r/2)$. It is interesting to note that r_1 tends toward r when r is small enough, which transforms the equations of the stereographic projection into those for the azimuthal equidistant projection. This similarity is clearly shown in figure 1 where the stereographic map overlays the azimuthal equidistant map, as we are treating small domains.

3. Application of the ring diagram analysis

We have applied ring diagram analysis to 3D data cubes corresponding to about 27 hours (1664 min) in time and to different field sizes. The starting point is an equidistant (X,Y) grid. A projection transformation is applied to each point of the grid, resulting in a heliographic coordinate, which in turn is used to find the corresponding position in the Doppler map by taking into account the apparent semi diameter and the solar inclination toward the Earth (B_0 angle). These positions are followed in time by compensating for the differential solar rotation. This remapping/tracking part of the technique is described in [2].

We have used all projections described above to calculate two daily flow maps at 189 positions of the solar surface, using GONG data from 02/01/2002 and 28/01/2002. The results have been obtained using a customized GONG++ ring diagram pipeline. We have applied the four projections with the standard patch size ($15^\circ \times 15^\circ$) and with patches which are four times bigger ($30^\circ \times 30^\circ$). The results are presented in figures 2 and 3.

4. Discussion and Conclusions

Figure 2 presents the velocity field for two different days and three different depths for the four studied projections using the standard ($15^\circ \times 15^\circ$) patch sizes. The difference between the projections are most prominent close to the limb, where the flow errors are quite large due to foreshortening. Deeper layers show the most prominent differences in the flows. However, ring diagram analysis is not very efficient at deep layers as low degree modes are not well enough identified because of the small size of the patches. Also, surface layers are suffering from bad estimations of the inversion kernels, which makes the errors significant in these layers. Moreover, most of the differences between the flows that are calculated using the four considered projections are due to both the accuracy of the technique and the observations. This result has been expected as all the projections result in nearly the same geometrical map within an area of the size of the standard patches (see figure 1), and are all based on great circles.

Figure 3 shows the velocity field for the two days and the three depths for the four studied projections when using the larger ($30^\circ \times 30^\circ$) patch sizes. In this case, the differences between the projections are more significant than those for the standard patch size. However, the results are smoother because the treated area is bigger. The differences at the limb, the surface and the deep layers are mainly due to the same errors, as mentioned above for the standard patches.

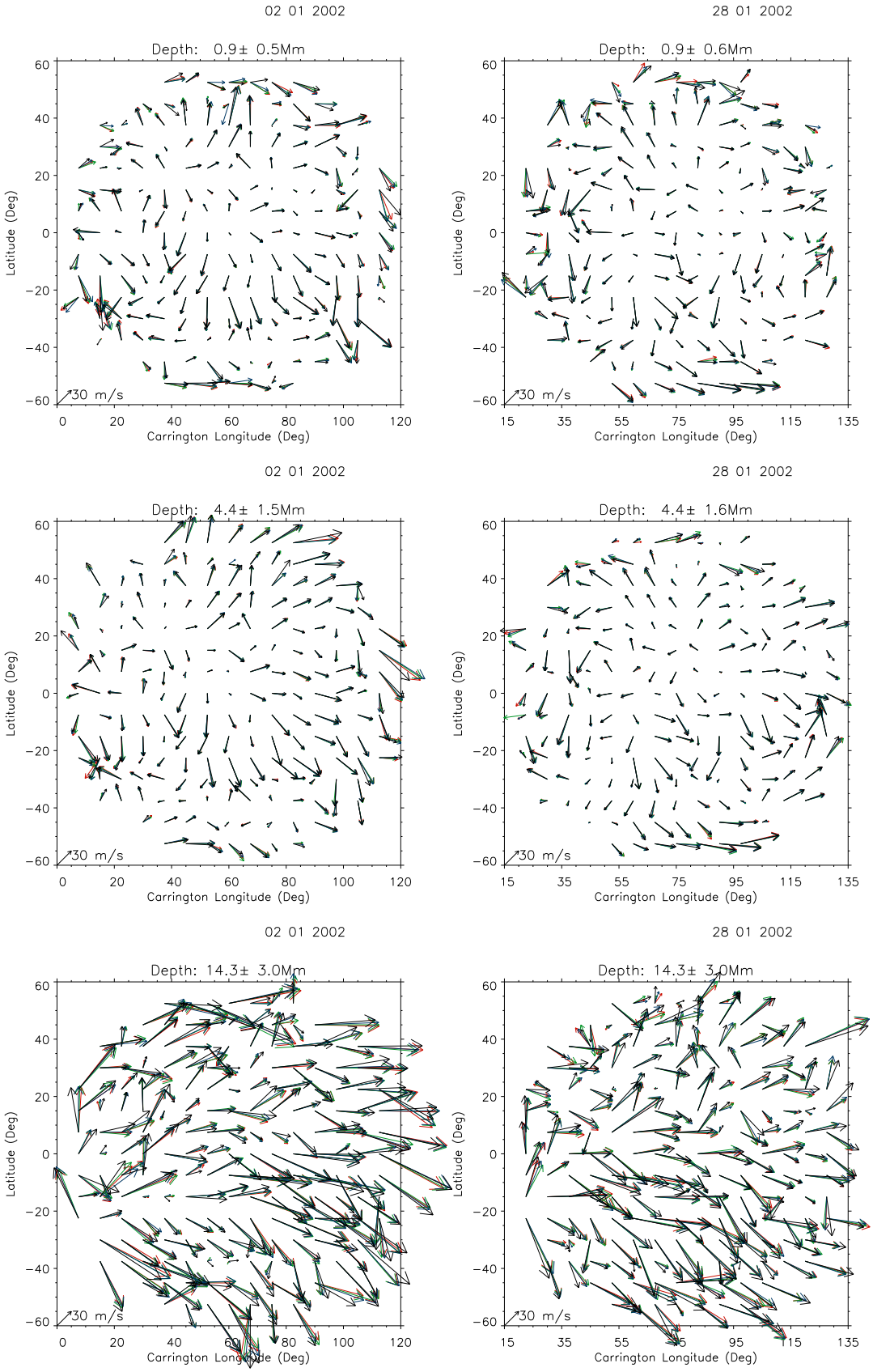

Figure 2. Daily flow maps constructed for two different days and three different depths by ring diagram analysis of $15^\circ \times 15^\circ$ patches. The different colors correspond to the following mappings: transverse equidistant cylindrical (red), azimuthal equidistant and stereographic (green and blue, overlayed), gnomonic (black).

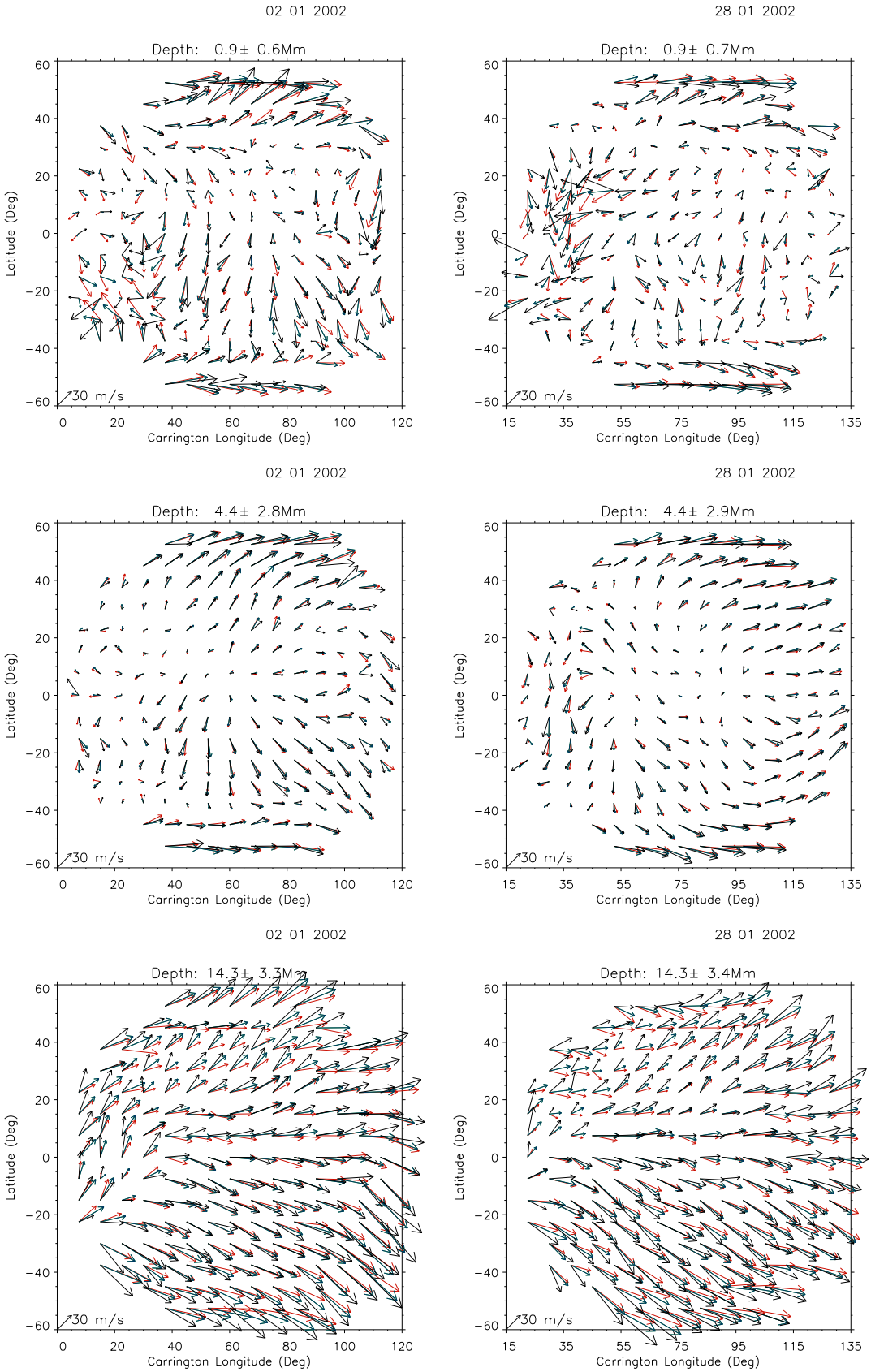

Figure 3. Same as figure 2 for 30° × 30° patches.

Moreover, the deviations observed with big patches may be due to the fact that the ring diagram technique uses a plane wave approximation, which is only valid for areas of limited size. In addition to these technical errors, the gnomonic projection seems to deviate most significantly in comparison to the other projections. This could be due to the fact that there is a stronger difference of this map compared to the others when the big patch size is considered (see figure 1). Indeed, the gnomonic projection produces relative distance distortions in the two directions as large as 6.75% in the limit of $30^\circ \times 30^\circ$ patches, whereas the maximum of the relative distortion for small patches is about 1.73%.

As a conclusion, the azimuthal equidistant, the cylindrical transverse, the stereographic and the gnomonic projections produce very similar results for the horizontal flows when applied to map areas with the standard size of ring diagram analysis patches. A bigger area results in more prominent differences, especially for the gnomonic projection.

References

[1] Hill F., 1988, *ApJ*, 339, 996

[2] Cobard T., Toner C., Hill F., Hanna K. D., Haber D. A., Hindman B. W., Bogard R. S., 2003, in SOHO 12 / GONG+ 2002. Local and global helioseismology: the Present and Futur, ASP 517, p. 255

[3] Bogart R. S., Sa L. A. D., Duvall T. L., Haber D. A., Toomre J., Hill F., 1995, Proc. Fourth SOHO Workshop: Helioseismology, ESA SP- -376, Vol. 2, p.147

[4] Haber, D.A., Hindman, B.W., Toomre, J., Bogart, R.S., Larsen, R.M. and Hill, F. 2002, *ApJ*, 570, 255.

[5] Gonzalez Hernandez I., Komm, R., Hill, F., Howe, R., Corbard, T., Haber, D.A., 2006, Astrophys. J 638, 576

[6] Haber D., Toomre J., Hill F., Gough D., 1995, in GONG'94: Helio- and Asteroseismologyfrom the Earth and space, ASP 76, P. 272

[7] Snyder J.P., Yang Q. H., Tobler W. R., 2000, Technology industrial arts, P. 367